Resistance minimum in LaAlO3/Eu1-xLaxTiO3/SrTiO3 heterostructures

Lebedev, N.; Huang, Y.; Rana, A.; Jannis, D.; Gauquelin, N.; Verbeeck, J.; Aarts, J.

Resistance minimum in LaAlO$_3$/Eu$_{1-x}$La$_x$TiO$_3$/SrTiO$_3$ heterostructures

N. Lebedev,[1,*] Y. Huang,[2] A. Rana [ORCID],[3,4] D. Jannis [ORCID],[5] N. Gauquelin [ORCID],[5] J. Verbeeck,[5] and J. Aarts [ORCID][1,†]

[1]*Huygens-Kamerlingh Onnes Laboratory, Leiden University, P.O. Box 9504, 2300 RA Leiden, The Netherlands*
[2]*Van der Waals-Zeeman Institute, University of Amsterdam, Science Park 904, 1098 XH Amsterdam, The Netherlands*
[3]*Center for Advanced Materials and Devices, BML Munjal University (Hero Group), Gurgaon 122413, India*
[4]*MESA+ Institute for Nanotechnology, University of Twente, P.O. Box 217, 7500 AE Enschede, The Netherlands*
[5]*Electron Microscopy for Materials Science, University of Antwerp, Campus Groenenborger Groenenborgerlaan 171,*
2020 Antwerpen, Belgium

In this paper we study LaAlO$_3$/Eu$_{1-x}$La$_x$TiO$_3$/SrTiO$_3$ structures with nominally $x = 0, 0.1$ and different thicknesses of the Eu$_{1-x}$La$_x$TiO$_3$ layer. We observe that both systems have many properties similar to previously studied LaAlO$_3$/EuTiO$_3$/SrTiO$_3$ and other oxide interfaces, such as the formation of a two-dimensional electron liquid for two unit cells of Eu$_{1-x}$La$_x$TiO$_3$; a metal-insulator transition driven by the increase in thickness of the Eu$_{1-x}$La$_x$TiO$_3$ layer; the presence of an anomalous Hall effect when driving the systems above the Lifshitz point with a back-gate voltage; and a minimum in the temperature dependence of the sheet resistance below the Lifshitz point in the one-band regime, which becomes more pronounced with increasing negative gate voltage. However, and notwithstanding the likely presence of magnetism in the system, we do not attribute that minimum to the Kondo effect, but rather to the properties of the SrTiO$_3$ crystal and the inevitable effects of charge trapping when using back gates.

I. INTRODUCTION

At oxide interfaces, mainly based on the SrTiO$_3$ (STO), two-dimensional electron liquids (2DELs) are easily formed. These systems have significant freedom of manipulating various magnetotransport properties by applying a gate voltage. One outstanding feature, of interest for spintronics applications, is the tunability of the spin polarization or magnetism. Its signature, the anomalous Hall effect (AHE), was extensively studied in the past decade in various STO-based structures [1–9]. It was shown, in particular, that the AHE can be completely switched off by a gate voltage, at least in some of these structures. The switching point is strongly connected to the so-called Lifshitz transition [10], which separates two regimes with only the $3d_{xy}$ band occupied, leading to single-band transport, or with involvement of both the $3d_{xy}$ and $3d_{xz/yz}$ bands. The latter regime coincides with the presence of AHE and, therefore, with the occurrence of spin polarization [1–5,10]. These are absent in the one-band regime, but there a nonmonotonous temperature dependence of the sheet resistance, with a pronounced minimum, has been observed. This behavior has been attributed to the presence of a Kondo regime [2,4]. For STO(001)-based interfaces, it has been proposed that different coupling between the localized magnetic moments and the $3d_{xy}$ and $3d_{xz/yz}$ electrons, due to the different orbital orientation relative to the interface plane, can explain various magnetotransport properties of STO struc-

tures, including a gate-tunable Kondo-like minimum, AHE, and behavior of the in-plane magnetoresistance (MR) [1,11]. Nevertheless, the mechanism for invoking Kondo-like effects is still a matter of debate. It was argued that enhanced spin-orbit coupling (SOC) at low temperature can produce some features of the in-plane MR which previously have been interpreted as supporting Kondo behavior [12].

This work aims to study the gate-tunable magnetic interactions. We choose as a starting point the well-known delta-doped system LaAlO$_3$/EuTiO$_3$/STO (LAO/ETO/STO). This system, where the 2DEL presumably forms at the interface between the ETO and the LAO, is reported to be ferromagnetic [2,13] and to exhibit both tunable AHE and Kondo-like behavior, and even superconductivity. Bulk EuTiO$_3$ is an antiferromagnetic band insulator [14–20]. The oxidation state of Eu is Eu^{2+}; therefore Ti is in the tetravalent state and does not contribute to the magnetization. However, doping the bulk with La will lead to the development of ferromagnetism [21,22], because La is in the La^{3+} state, and the doping introduces electrons into the conduction band of the $3d$ t_{2g} states of the Ti, turning ETO into a ferromagnetic metal [21,22]. In this paper, to understand the role of La doping (or diffusion) in the magnetic interactions, we also investigated nominally nonmagnetic LAO/STO and LAO/Eu$_{0.9}$La$_{0.1}$TiO$_3$/STO (LAO/ELTO/STO). We find a gate-tunable AHE by inserting two unit cells (2 u.c.) of ETO or ELTO, and we find a transition between tunable AHE and Kondo-like regimes. However, unlike the AHE, the Kondo-like regime seems to be present even at zero gate voltage, although the dip becomes more pronounced at finite negative voltages. We come to the conclusion that the

*lebedev@physics.leidenuniv.nl
†aarts@physics.leidenuniv.nl

voltage-dependent Kondo-like resistance behavior is not a sign of magnetic interactions, but most likely the result of the interplay between the electron trapping mechanism and the temperature dependence of the STO permittivity, the carrier concentration, and various scattering mechanisms. The combination of these effects leads to more effective back gating at low temperatures and therefore to an increase in resistance which has little to do with magnetic scattering.

II. EXPERIMENTAL DETAILS

The oxide structures were grown by pulsed laser deposition (PLD) on TiO_2-terminated (001)-oriented STO. In the literature, two types of targets have been used to grow ETO: the pyrochlore material $Eu_2Ti_2O_7$ [13,23–27] and the perovskite material $EuTiO_3$ [28–31]. In this paper, we choose to work with the latter. The PLD targets for ETO and $Eu_{0.9}La_{0.1}TiO_3$ were fabricated from sintered and pressed powders. The LAO target was commercially purchased. The nominal La doping was chosen at 10% to ensure a significant difference between intentionally doped films and unintentional doping due to possible intermixing. However, as we will show in Sec. III A the resulting doping was different. Significant optimization of the growth parameters was required to obtain good growth. In order to prevent bulk conductivity of the STO due to oxygen depletion at the high growth temperatures, some oxygen in the PLD chamber is needed, but the oxygen pressure should not be too high; otherwise the ETO and ELTO films become amorphous or form the pyrochlore structure.

Based on the optimization of the growth parameters we chose a fluence of $1.54 \, J/cm^2$ for ETO and ELTO and spot size $1.38 \, mm^2$. For LAO a growth fluence of $1.3 \, J/cm^2$ and a spot size of $1.76 \, mm^2$ were used. The temperature was set at $800 \, °C$, and the nominal pressure, consisting of a $1:1$ mix of $Ar:O_2$, was set at 1×10^{-4} mbar. The maximum thickness of the $Eu_{0.9}La_{0.1}TiO_3$ layer was fixed at 4 u.c. Above that value, growth of the $Eu_{0.9}La_{0.1}TiO_3$ films results mostly in an amorphous reflection high-energy electron diffraction (RHEED) pattern, meaning that the crystalline diffraction spots are lost. Still, that thickness is enough to study delta-doped LAO/STO structures. The following samples were grown (the numeral denoting the number of unit cells): LAO(10)/ETO(t)/STO (with $t = 2, 3, 4$), LAO(10)/ELTO(t)/STO (with $t = 2, 4$), ELTO(4)/STO, ETO(4)/STO, and LAO(10)/STO.

Figure 1(a) shows the RHEED intensity variations during growth for both ETO and ELTO, which are quite similar. Oscillations are clearly visible for the ELTO(4)/STO and ETO(4)/STO samples (black and red lines). The RHEED pattern for ETO(4)/STO shows additional lines at the 1/2 position between the main lines for films with $t > 2$ u.c. (see inset in Fig. S1(b) of the Supplemental Material [32]); such lines have been observed for stoichiometric $Eu_{0.9}La_{0.1}TiO_3$ films [33]. The STO surface steps can be clearly seen in the atomic force microscopy (AFM) scan before and after growth (see Supplemental Fig. S1), but the edges become more rough than on the bare STO surface. Moreover, there are islandlike features in the topography of the film. During the growth of LAO, clear oscillations are seen when growing directly on STO [blue line in Fig. 1(a)]. Note that we had to increase the RHEED intensity during the growth of LAO
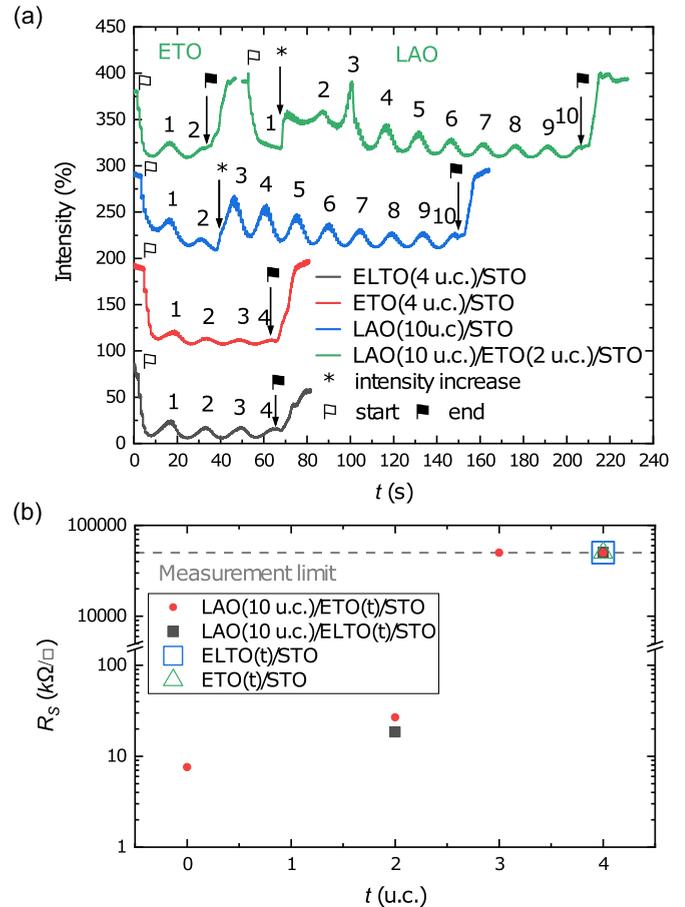
FIG. 1. (a) RHEED intensity monitoring during the growth of (from bottom to top) ELTO(4)/STO, ETO(4)/STO, LAO(10)/STO, and LAO(10)/ETO(2)/STO. All traces are consecutively offset by 100% for clarity. Special symbols denote the start and end of the deposition of each material, as well as (in two cases) a manual increase in intensity when starting LAO growth. (b) The thickness dependence of the sheet resistance R_S at 300 K for E(L)TO and LAO/E(L)TO samples grown on STO. Note the metal-to-insulator transition above 2 u.c.

layers. The RHEED pattern shows a transition from two-dimensional (2D) growth to 3D growth [inset in Supplemental Fig. S1(c)], most likely due to the low oxygen pressure. A clear underlying STO step pattern can be seen in the AFM scan in Supplemental Fig. S1(c). This is different when the LAO layer is grown on ETO or ELTO films. In Fig. 1(a) (green line) the first two oscillations during LAO growth become less pronounced, and their intensity decreases with the increase of the ETO or ELTO layer thickness. The thickness of the LAO layer was determined from the number of pulses for a single period of oscillations and, strictly speaking, can vary between 8 and 10 u.c. That variation is not crucial for the conductivity of $LAO/EuTiO_3/STO$, in contrast to the thickness of the ETO layer [13]. The LAO layer grown on the ETO or ELTO also shows 3D features in the RHEED pattern, but the 2D features are more pronounced [inset in Supplemental Fig. S1(d)]. The underlying topography of ETO or ELTO films can still be seen after depositing the LAO layers as shown in Supplemental Fig. S1(d). After growth, the
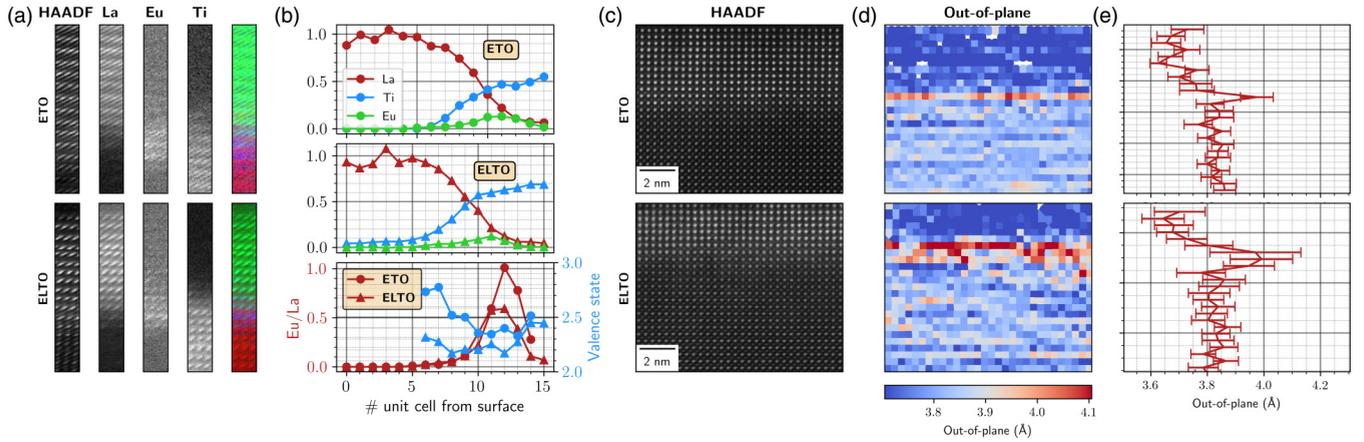
FIG. 2. (a) High-angle annular dark-field imaging of the ETO (upper panels) and the ELTO (lower panels) samples. The presence of La, Eu, and Ti when crossing the interface is indicated. The color plots show La in green, Eu in purple, and Ti in red. (b) EELS analysis of the La, Eu, and Ti content as a function of unit cell distance from the surface for ETO (upper panel) and ELTO (middle panel). The lower panel shows the Eu-to-La ratio (left-hand scale) and the Eu valence state (right-hand scale) for both samples. (c) HAADF imaging of the interface region for ETO and ELTO. (d) and (e) Analysis of the out-of-plane lattice constant from the image in (c). LAO/ETO/STO is denominated as ETO, and LAO/ELTO/STO is denominated as ELTO.

magnetotransport properties were measured in van der Pauw geometry in a physical property measurement system (PPMS) from Quantum Design with home-built insert for performing gating experiments. Two samples of LAO(10)/ETO(2)/STO and LAO(10)/ELTO(2)/STO were subsequently analyzed by scanning transmission electron microscopy (STEM), electron energy loss spectroscopy (EELS), and high-angle annular dark-field (HAADF) imaging.

The basic behavior of our samples is similar to that of the ones studied in Refs. [2,13]. In particular, both our LAO/ETO/STO and our LAO/ELTO/STO show a metal-insulator transition (MIT) as a function of E(L)TO thickness around 2 u.c. [Fig. 1(b)], which is in agreement with the results of Ref. [13]. Hereinafter, we will refer to the two conducting samples, LAO(10)/EuTiO$_3$(2)/STO and LAO(10)/Eu$_{0.9}$La$_{0.1}$TiO$_3$(2)/STO, as LAO/ETO/STO and LAO/ELTO/STO, respectively. The fact that uncapped ETO and ELTO samples were insulating above 2 u.c. indicates that La doping of the E(L)TO layer in our films is not the driving mechanism of the MIT [21,22]. At room temperature, LAO/STO has a lower sheet resistance R_S than LAO/ELTO/STO, which in turn is lower than that of LAO/ETO/STO.

III. RESULTS

A. STEM characterization

Extensive HAADF and EELS analysis [Figs. 2(a) and 2(b)] revealed clear intermixing of La and Eu in the ETO sample. The sample shows a higher Eu-to-La ratio, which means less La, than the ELTO sample. This is to be expected, but the fact remains that the difference between the two samples is smaller than was intended. For both samples, the effective ELTO layer becomes 3 u.c. thick due to diffusion, and the Ti diffuses 5 u.c. inside the LAO. We also note a higher diffusion of Eu inside the LAO for ETO than for ELTO. This is evident from the presence of a higher concentration gradient in LAO/ETO/STO. Some Eu diffuses inside the LAO, where

it is present as Eu^{3+}, which is nonmagnetic. Overall, the Eu valence states in the ETO and ELTO layers are Eu$^{2.36+}$ and Eu$^{2.3+}$, respectively [see the blue line in the bottom panel of Fig. 2(b) and also Supplemental Fig. S2]. Thus the doping layers appear to resemble each other quite closely. However, Eu is distributed rather uniformly in the ELTO layer, which is not the case in the ETO layer, where Eu is concentrated close to the interface. That may lead to a higher concentration of magnetic moments in the first layer next to the interface of ETO and STO. HAADF imaging [Fig. 2(c)] was used to extract lattice parameter variation for both samples, which is presented in Figs. 2(d) and 2(e). In both cases, the films are relaxed in plane, as shown in Supplemental Figs. S2(c)–S2(f). We can notice an expansion of the out-of-plane lattice parameter within 1 u.c. for ETO while it is present over 3 u.c. in the ELTO sample.

B. Magnetotransport properties at zero gate voltage

Before applying gate voltages, we analyze the temperature dependence of the magnetotransport properties for the three conducting samples. The introduction of the thin sheet of Eu$_{0.9}$La$_{0.1}$TiO$_3$ also changes the temperature dependence of R_S: The LAO/STO sample exhibits a monotonous decrease down to 3 K, whereas the delta-doped samples show an upturn below 10 K [Fig. 3(a)]. Such a change in $R_S(T)$ has been reported in Ref. [13] and was attributed to a possible Kondo effect [13,34]. The behavior of the MR is described in the Supplemental Material.

The behavior of the Hall coefficient is of more significance in the context of this work. Below 100 K, the Hall coefficient R_H develops a nonlinearity in high fields, indicating the onset of two-band transport [10] (see the Appendix, Fig. 7). Furthermore, below 10 K, there is also a low-field nonlinearity in the magnetically doped samples. This indicates the presence of an anomalous Hall effect (AHE), which has often been observed and analyzed [2,3,8,10] in order to determine the carrier concentrations n_i and mobilities μ_i of both bands,
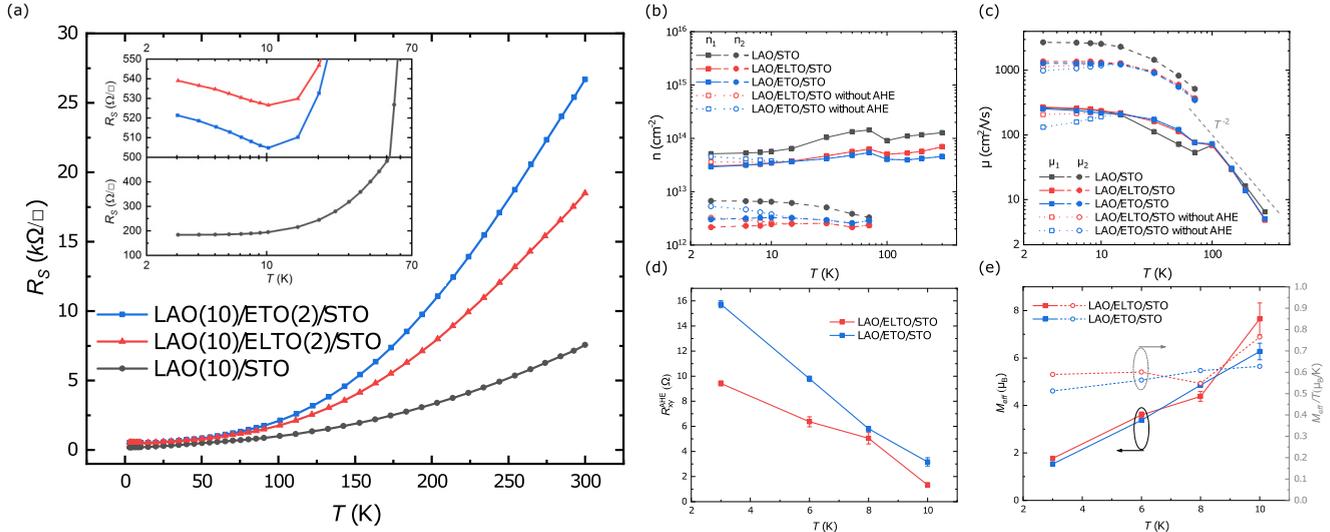
FIG. 3. (a) Temperature dependence of R_S for samples with and without an E(L)TO interlayer. The inset shows details of the low-temperature region. For the LAO/STO and the LAO/E(L)TO/STO samples, temperature dependences are given for (b) the carrier concentrations n_i, (c) the mobilities μ_i, (d) the anomalous Hall coefficient R_{xy}^{AHE}, and (e) values of M_{eff} (solid symbols) plus the ratio M_{eff}/T ratio (open symbols). They were taken from fitting as described in the Appendix. Note that n_i and μ_i are given both with and without correction for the AHE when appropriate.

and the anomalous Hall coefficient R_{xy}^{AHE}. Our analysis uses a substraction method described earlier in Ref. [8]. Details are included in the Appendix, where we also introduce an effective magnetic moment M_{eff} to take account of the presence of the AHE. The extracted values for n_i, μ_i, R_{xy}^{AHE}, and M_{eff} are shown in Figs. 3(b)–3(e). Also shown are the values for n_i and μ_i when no AHE is taken into account. We see that in the one-band region, the mobility of the samples roughly follows a T^{-2} dependence in the temperature range 150–50 K [Fig. 3(c)]. The temperature dependence above 150 K is often ascribed to longitudinal optical phonon scattering, and the origin of T^{-2} mobility dependence is usually attributed to electron-electron scattering [35,36]. As was mentioned above, the second band appears below 100 K. Some unphysical jumps are probably related to the low carrier concentration of the second band leading to overestimating (underestimating) the carrier concentration (mobility) for both types of carriers. Overall it is clear that the trend is an increase of $\mu_{1,2}$ towards low temperatures with saturation below 10 K and a continuous although small decrease of n_1. The saturation of the mobility at a low-temperature limit is most likely due to the interface, to ionized donors, and to ionized impurity scattering [35]. In the fit without the AHE, with decreasing temperature we see an increase in carrier concentration and a decrease in mobility for the magnetically doped samples below 10 K. However, when accounting for the AHE, the fits become consistent with the general trend of LAO/STO. The AHE grows when lowering the temperature [Fig. 3(d)], but we see that the fit parameter M_{eff} decreases almost linearly with temperature as can be seen better from the ratio M_{eff}/T [Fig. 3(e)]. This is quite counterintuitive. If M_{eff} would simply represent the saturation magnetization of a ferromagnetically ordering interface, the trend should be opposite. Since an ordering temperature of around 10 K is expected, this points to a different interpretation of M_{eff}, which may not be surprising, since the AHE

depends on more than the magnetization alone, with SOC to start with. It does not affect the determination of R_{xy}^{AHE} and the shape of the function used.

C. Gate tuning of the magnetotransport properties

Next, for all samples, we measure the temperature dependence of R_S from 100 K down under a series of applied gate voltages V_G, starting at $+150$ V and going down to -150 V in a number of steps. Voltages were always set at 3 K. After setting the voltage to the target voltage, the temperature was increased to 100 K, and R_S was measured during cooldown. When reaching 3 K, the voltage was set to the next (lower) value. We observe the development of the minimum in $R_S(T)$ below $+25$ V in magnetically doped samples [Figs. 4(a) and 4(b)], which becomes more pronounced with increasingly negative V_G. That particular feature in the temperature dependence is often attributed to Kondo-like behavior [2], which might well be connected to the magnetism of the doping layers. However, and surprisingly, we see quite similar behavior in nominally nondoped LAO/STO samples [Fig. 4(c)], where we do not observe the AHE. These are intriguing observations and a reason to look more closely at the actual effects of the magnetic interlayers.

For this we studied the combined temperature dependence and gate dependence of the AHE in doped samples below 10 K, which also entails determining n_i and μ_i. Again, the voltage was first swept at 3 K, and then the temperature was increased to 15 K. The measurements were performed during cooldown. At each temperature and voltage point, the magnetic field was varied. Before changing the temperature or voltage, the field was brought to zero in an oscillating manner. In order to represent both temperature and gate voltage dependence, we use a false-color plot, where the colors represent the values of the various parameters. This is done in Figs. 5(a)–5(e) for LAO/ETO/STO.
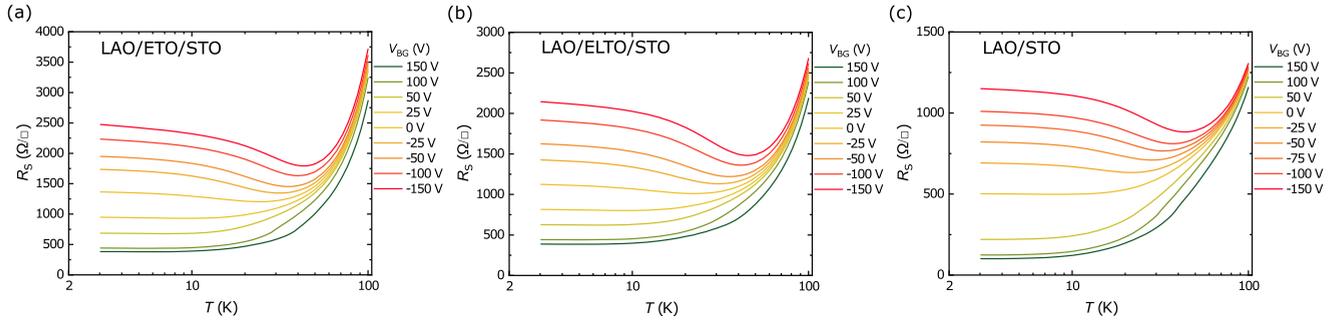
FIG. 4. Temperature dependence of the sheet resistance R_S for different applied gate voltages in a range between $+150$ and -150 V, as indicated, for (a) LAO/ETO/STO, (b) LAO/ELTO/STO, and (c) LAO/STO.

Before describing the results, we need to make one caveat. By not increasing the temperature to 100 K, as was done for the data of Fig. 4, and also below in Fig. 6, we actually prepare the sample differently, in particular, with respect to the number of trapped versus free carriers. This is because detrapping cannot fully be avoided, even if staying below the temperature where the STO undergoes a crystallographic phase transition. The trends shown in Fig. 5 are relevant to the narrative, but numbers cannot be related one to one with those of the other experiments. Looking then at those trends, the results are similar to those of previous AHE studies in the two-band regime in the oxide interfaces [2,5,10,37]. We find a Lifshitz point [10] located near 25 V as can be seen from the behavior of n_2 [Fig. 5(b)], where carriers of the second type disappear below that voltage. Unlike the carrier concentration and mobility of the low-mobility carriers [Figs. 5(a) and 5(c)], the carrier concentration and mobility of the high-mobility carriers [Figs. 5(b) and 5(d)] are less sensitive to a change in temperature. On the other hand, the change in voltage affects n_i and μ_i much more strongly. The behavior is qualitatively the same for both samples; numbers for LAO/ELTO/STO can be found in Supplemental Fig. S3. The AHE [Fig. 5(e)] is not present in the region where two-band behavior is absent, as would be expected in the picture where the AHE is simply controlled by the second type of carriers [1]. However, R_{xy}^{AHE} also disappears above 10 K. That can be due to vanishing of the magnetization [2], vanishing of the spin-orbit coupling [8], or both. Indeed we see the signature of weak antilocalization (WAL), indicative of spin-orbit coupling in the low-field MR in all samples. Note that the MR is strongly affected by changes in gate voltage and temperature (see Supplemental Fig. S5). At the same time, the AHE coefficient is higher in the ETO-based sample than in the ELTO-based sample. Apart from that, the gate voltage dependence and temperature dependence of the AHE coefficient for LAO/ELTO/STO [Fig. 5(f)] are similar to those for LAO/ETO/STO. Some notes on the mechanism of the AHE can be found in the Supplemental Material [32] and Refs. [38–40]. Furthermore, the field dependence of the Hall coefficient of the LAO/STO sample at 3 K for various voltages (Supplemental Fig. S7) shows no low-field nonlinearity, unlike the magnetically doped samples. Here, we point out that the upturn in $R_S(T)$ sets in below the same voltage where R_{xy}^{AHE} and n_2 fall to zero in the magnetically doped samples, which is 25 V. So, magnetic doping significantly affects the spin-polarized phase of the two-dimensional electron gas (2DEG) in the two-band regime, where the moment was

argued to be ferromagnetically coupled with $3d_{xz/yz}$ electrons, but seems not to have any qualitative effect on the Kondo-like (one-band) regime, where the moment has been claimed to be antiferromagnetically coupled with $3d_{xy}$ electrons [1,11].

To understand the nature of this behavior, we measured the temperature dependence of the sheet resistance $R_S(T)$ for all three samples at -100 V in a larger temperature range (from 100 K downward) and performed magnetotransport measurements (both MR and Hall) during cooldown at a few temperatures in order to find carrier concentrations and mobilities at this gate voltage. As can be seen in Fig. 6(a), the samples show somewhat lower values of the sheet resistance when compared with Fig. 4 but follow the same trend with a minimum around 30–40 K and saturationlike behavior below 10 K. The extracted carrier concentrations [Fig. 6(b)] from the magnetotransport data showed a constant decrease in carrier density with decreasing temperature. This is similar to the behavior of the carrier concentration of the low-mobility carriers without back-gate voltage, but here it is also observed for the high-mobility carriers, and especially strong below 10 K. At the same time, the mobility [Fig. 6(c)] increases at first with decreasing temperature, but below 40 K it is saturated, similar to the temperature dependence without applied back-gate voltage, and can be described by the same scattering picture. Important to note is that the change in the temperature dependence of the mobility happens around the temperature corresponding to the minimum in the sheet resistance. To illustrate how the change in carrier concentrations and mobilities affects the temperature dependence of the sheet resistance, we plot conductance $G_{xx} = 1/R_S$ and band conductances $en_i\mu_i$ in Fig. 6. Finally, a remark can be made as to the similarities and differences between Fig. 5 and Fig. 6: The values for n_1 and μ_1 are very similar, while, in particular, n_2 is still measurable at 10 K after the procedure followed in Fig 6 but already zero for the procedure followed in Fig. 5.

IV. DISCUSSION

The results shown here are consistent with studies of LAO/ETO/STO in Refs. [2,13,37]. As in the earlier studies, we observe the MIT, the tunable AHE, the appearance of a resistance minimum, and also WAL behavior. The AHE is the possible signature of ferromagnetism. Indeed, x-ray magnetic circular dichroism (XMCD) data seem to support that picture [2,13]. Nevertheless, bulk ETO is an antiferromagnet [14–20]. It is also isostructural to STO, and therefore
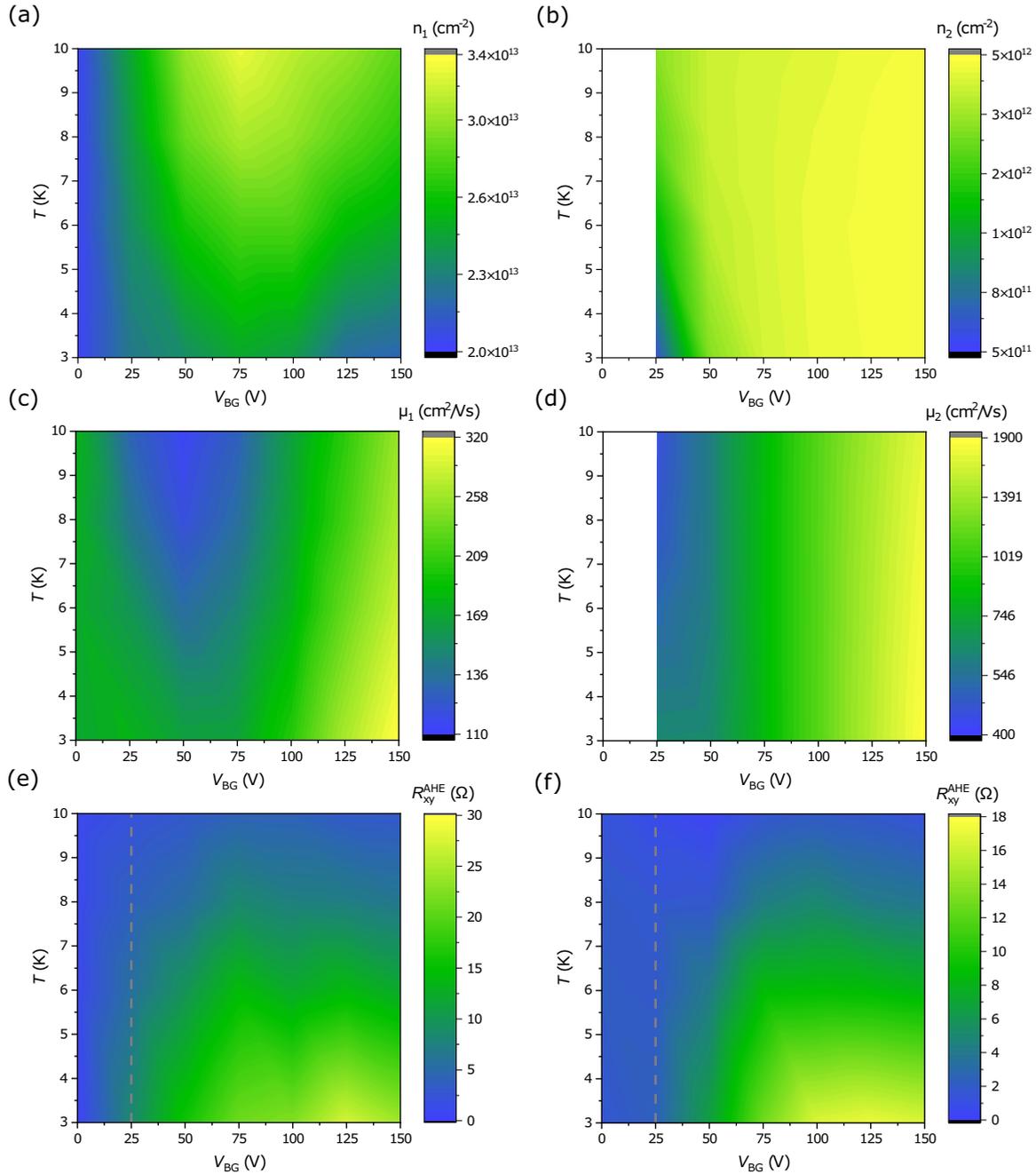
FIG. 5. Temperature and back-gate voltage dependence of (a) and (b) carrier concentrations, (c) and (d) mobilities, (e) the anomalous Hall coefficient for the LAO/ETO/STO sample, and (f) the anomalous Hall coefficient for the LAO/ELTO/STO sample. Gray dashed lines in (e) and (f) indicate the Lifshitz transition. Note that at 10 K there is still a bit of nonlinearity in the Hall signal indicating two-band transport. For all quantities, the color scale gives the full range of their values. The same colors therefore do not mean the same values.

stoichiometric ETO should remain antiferromagnetic, when grown on STO [41]. At the same time, experiments revealed that antiferromagnetism only occurs for postannealed PLD films [26,27] and films grown by molecular beam epitaxy (MBE) [41]. Here, we used PLD films without annealing, which can become ferromagnetic [23,26–28] because of either the formation of oxygen vacancies [27,42] or a longer out-of-plane lattice constant, which leads to a bigger lattice volume [23,26,43]. The films tend to be ferromagnetic if the ratio between the out-of-plane constant and the in-plane constant is larger than 1.02 or less than 0.99. Due to large

error bars, we cannot estimate this ratio precisely, but our films may be on the edge of a ratio of 1.02 [43]. The crystallinity of our films allows us to exclude amorphization of ETO as the driving mechanism for the transition to a ferromagnetic state [44]. The doping with La [21,22,42,45] can also turn ETO into a ferromagnetic metal. The observed MIT and its weak sensitivity to the La content indicate that the occurrence of the AHE has a more complicated origin than just being due to ferromagnetism induced by off-stoichiometry in the ETO layer. Formally, however, that scenario is hard to exclude due to intermixing in samples. As it seems that we overshoot the
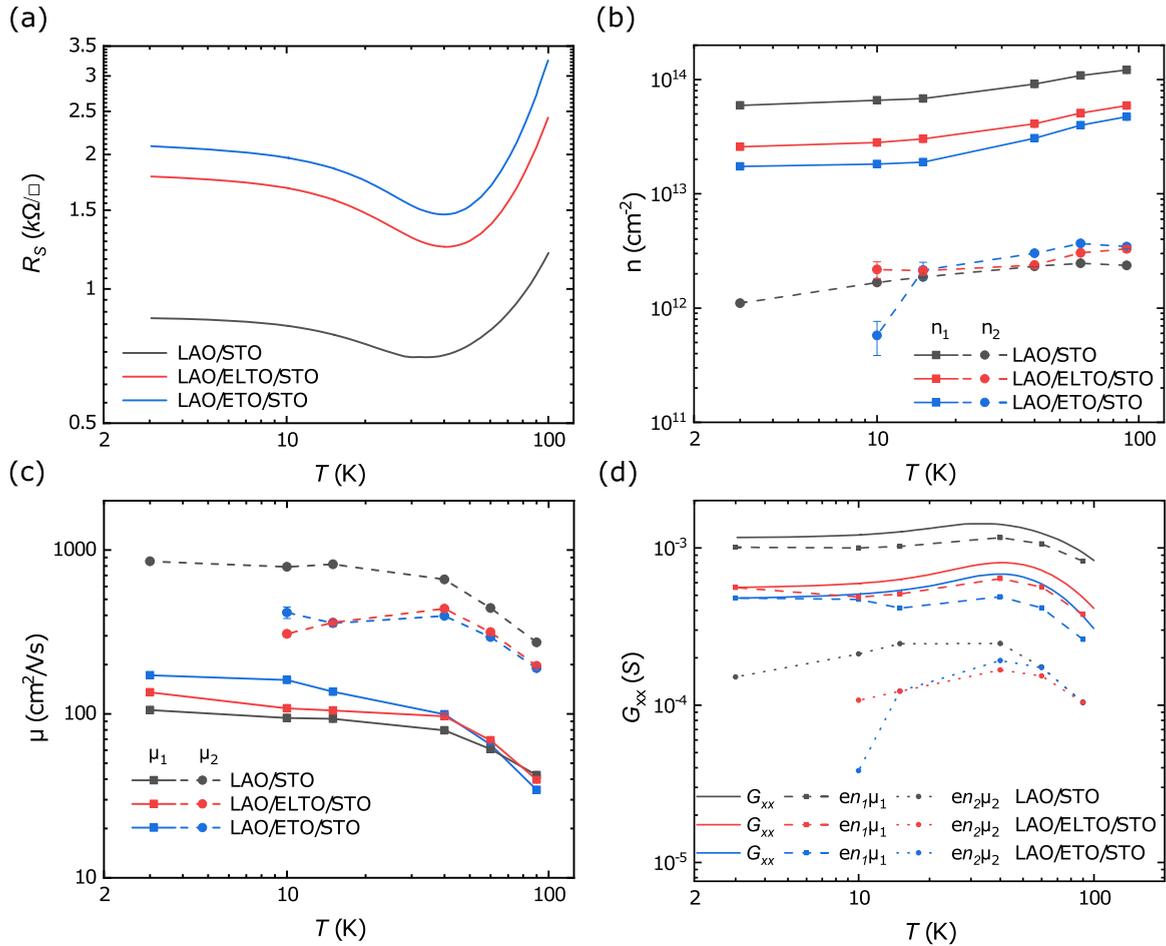
FIG. 6. Measurements at a gate voltage of -100 V for all three samples. (a) The temperature-dependent sheet resistance $R_S(T)$, (b) the carrier concentrations (note the disappearance of the second band below 10 K for the E(L)TO samples), (c) the mobilities, and (d) the conductance.

sweet spot of 10% for La doping, extra doping may weaken ferromagnetism [45].

The authors of Ref. [3] observed variations of the AHE with changes in the oxygen pressure used during the growth and proposed an indirect connection between the AHE and magnetism induced by Sr vacancies rather than with actual magnetic moments, including Ti^{3+} induced by oxygen vacancies. However, we used the same growth pressure for the nondoped LAO/STO sample and LAO/E(L)TO/STO, so the variation of Sr vacancies should not be too high from sample to sample. With the introduction of Eu doping, we observe an increase in the AHE magnitude, contrary to the findings of Ref. [3].

Another defect scenario concerns the formation of B-site cation defects in the LAO layer [9]. Indeed we observe in our samples the presence of Ti deeper in the LAO layer, which can give an additional contribution to the magnetism. References [1,11] proposed a ferromagnetic coupling of $3d_{xz/yz}$ with localized magnetic moments such as Ti^{3+} formed due to oxygen vacancies. That indeed can explain the observation of the AHE above the Lifshitz point, since skew scattering of $3d_{xz/yz}$ carriers seems to be a dominant contribution to the AHE in oxide interfaces in the two-band regime [1–4]. Nevertheless, it appears to be not straightforward to explain our

results on the tunable AHE. First, the AHE coefficient does not scale linearly with the mobility of high-mobility carriers as shown in the Supplemental Material. Second, and probably more importantly, our nondoped LAO/STO sample does not exhibit an AHE, despite the presence of $3d_{xz/yz}$ carriers. All in all, there are certainly multiple ways to induce magnetization and the AHE, but in our samples magnetic doping is the main one.

In the framework of magnetic doping, we have further indication that the picture of magnetic interactions based purely on the symmetry of orbitals does not hold, specifically from the data in the negative gate voltage range, where the AHE vanishes. The authors of Refs. [1,11] argued that the coupling between mobile $3d_{xy}$ electrons and localized magnetic moments is antiferromagnetic. Strong support for this picture came from the behavior of the negative in-plane MR. Above the Lifshitz point, the observed large drop of (negative) in-plane MR was attributed to the destruction of Kondo screening and the polarization of magnetic moments with applied field [1,11,46]. However, that picture was challenged by Diez *et al.* [12], who found that the negative in-plane MR survives up to 20 K, opposite to the expectations from the temperature-dependent Kondo picture. Furthermore, single-particle Boltzmann transport theory was

sufficient to reproduce the large negative MR by taking into the account finite-range electrostatic impurity scattering, the anisotropic Fermi surface above the Lifshitz transition, and the SOC.

In this paper, we also challenge the Kondo picture. At first sight, the minima at −100 V look very "Kondo-like." Fits to Kondo behavior are not, however, very convincing and, in particular, show no difference between the nominally nonmagnetic sample with LAO and the two samples which contain magnetic ions. The fits are given in Supplemental Fig. S8 (see also Ref. [47]). A different viewpoint came from experiments on the LAO/STO interface performed in Ref. [48]. They showed that the resistance minimum could be controlled by applying hydrostatic pressure and concluded that impurity scattering, the pressure, and the temperature dependence of the STO dielectric constant plus thermally activated charge trapping form the mechanism responsible for the resistance minimum. Our results on the back-gate voltage dependence of the sheet resistance can be interpreted in a somewhat similar manner. At negative gate voltages, the carrier concentration decreases in the whole temperature range, but down to 40–50 K the mobility is enhanced due to a decrease in electron-electron scattering. Taken together, that is the reason why we observe a decrease in the resistance down to a minimum temperature. However, with a further decrease in temperature, the change in mobility is much less steep due to various scattering mechanisms coming into play, as discussed in Sec. III B. Simultaneously, the decrease in the carrier concentration is continuous and especially pro-

nounced for the high-mobility carriers. It is not surprising, then, that in this region the sheet resistance starts to grow again.

Two mechanisms are responsible for the decrease in the carrier concentration. One is charge trapping [49,50], which is less effective at high temperatures than at low temperatures. Second and probably dominant here is the complex behavior of the electric permittivity of the STO single-crystal substrate at low temperatures. Indeed, at high temperatures above 40 K, the permittivity hardly changes with the applied electric field, but it does change significantly at lower temperature [51–53]. This means that the effect of back gating will be significantly more efficient in the low-temperature region. Furthermore, it is well known that back-gate experiments significantly affect the carrier concentration of the second type of carriers [10,54] at low temperatures. Below 10 K, a back-gate voltage depletes, or almost depletes, the second band; therefore the saturationlike behavior of R_S in this range can be explained by the much weaker change in the mobility and carrier concentration of the low-mobility carriers with temperature. Note that our results do not exclude the possibility of inducing the Kondo effect at the LAO/STO interface, but only indicate that in the back-gate geometry, other effects are dominant and responsible for the resistance minimum in the temperature dependence when it occurs after the application of a gate voltage. Top gating, or different experiments addressing spin screening, might be a better way to study the Kondo effect in the oxide heterostructures [55].
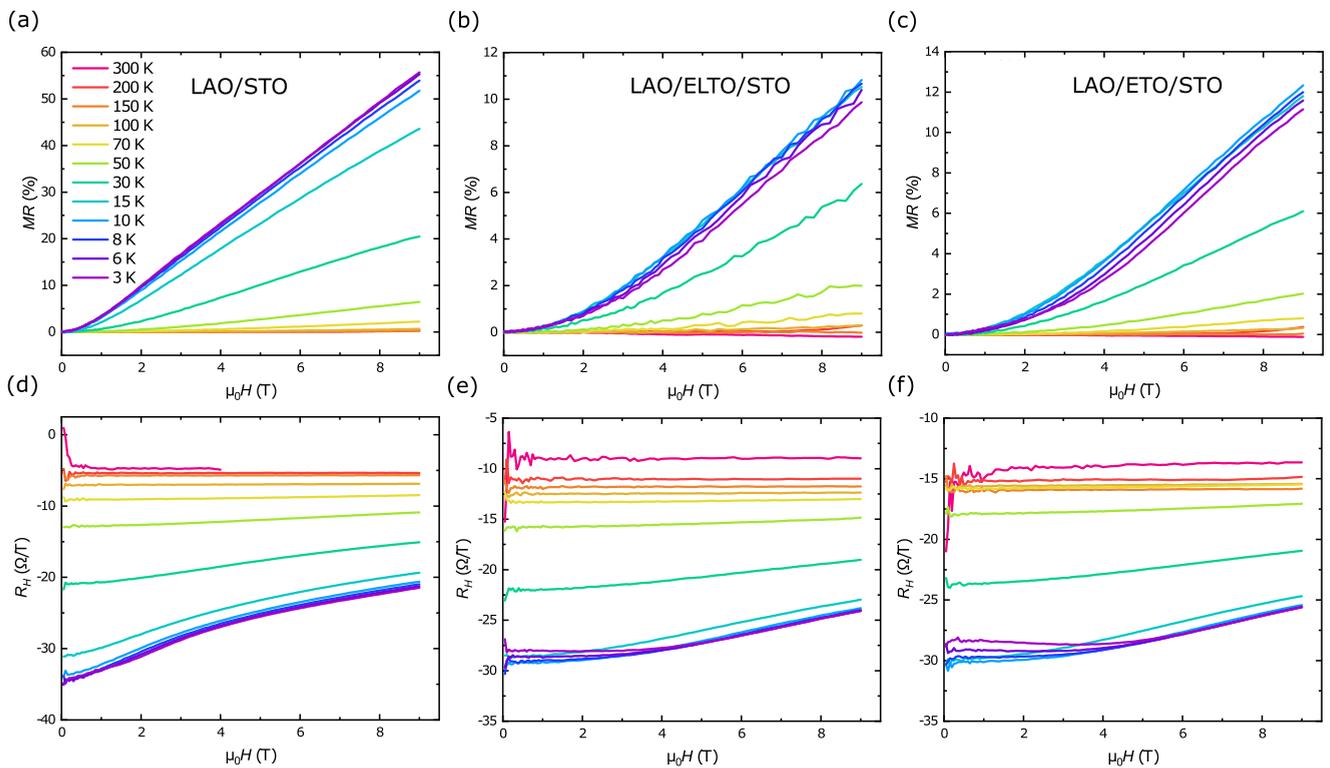
FIG. 7. Magnetoresistance (MR) with the field out of plane at different temperatures indicated by the colors for (a) LAO/STO, (b) LAO/ELTO/STO, and (c) LAO/ETO/STO. The Hall coefficient at different temperatures [same colors as in (a)–(c)] for (d) LAO/STO, (e) LAO/ELTO/STO, and (f) LAO/ETO/STO.

V. CONCLUSION

In conclusion, we have studied the LAO/STO interface with and without an inserted magnetic delta-doping layer of $Eu_{0.9}La_{0.1}TiO_3$ (either through La intermixing or intentionally). Our experimental results are mostly in agreement with previous research on these structures [2,13,37]. We observed that, despite extra lanthanum, the MIT happens at 2 u.c. Moreover, the AHE is indeed induced by inserting the 2 u.c. of ETO or ELTO and can be gate tuned. Furthermore, at negative back-gate voltages we find minima in the sheet resistance as a function of temperature. However, we do not attribute this to Kondo-like behavior, the presence of magnetic moments notwithstanding. In our interpretation, the minima rather arise from the temperature dependence of the carrier concentrations and mobilities of both conduction bands and are most probably due to spinless scattering mechanisms, charge trapping, and the complex temperature and electric field dependence of the STO permittivity.

APPENDIX

In LAO/STO, the value of the MR as a function of an applied magnetic field out of the plane of the sample continuously increases with decreasing temperature [Fig. 7(a)]. The high values of MR, around 50%, and the almost linear shape in high fields below 50 K point to spatial conductance fluctuation (see Refs. [56–63]). In the doped samples, the MR behavior is less monotonous; the MR increases only up to 10–12% until the temperature reaches 10 K [Figs. 7(b) and 7(c)]. Below that temperature, the MR decreases, tracing the upturn in the temperature dependence of R_S.

To analyze the data with respect to carrier densities n_i and mobilities μ_i in the presence of the AHE, we followed the subtraction method described in Ref. [8]. This method utilizes the small variation of the mobilities and concentrations in the temperature regime where the AHE is observed. Therefore, if we subtract the Hall resistance curve at higher temperature without the AHE from the Hall curve with the AHE at lower temperature, it will be possible to extract the AHE by fitting the resulting curve with the following equation:

$$\Delta R(B) = R_{xy}^{\text{AHE}} \tanh\left(\frac{M_{\text{eff}}\mu_B B}{k_B T}\right) + aB, \qquad \text{(A1)}$$

where a is the slope of residual ordinary Hall resistance. To increase the precision of the fit, we used the derivative of the subtraction result to determine the fitting range. The two-band analysis in a regime without AHE was performed using the fitting of the conductance tensor components (see, for instance, Ref. [64]).

[1] A. Joshua, J. Ruhman, S. Pecker, E. Altman, and S. Ilani, Proc. Natl. Acad. Sci. USA **110**, 9633 (2013).

[2] D. Stornaiuolo, C. Cantoni, G. M. De Luca, R. Di Capua, E. Di Gennaro, G. Ghiringhelli, B. Jouault, D. Marrè, D. Massarotti, F. Miletto Granozio, I. Pallecchi, C. Piamonteze, S. Rusponi, F. Tafuri, and M. Salluzzo, Nat. Mater. **15**, 278 (2016).

[3] F. Gunkel, C. Bell, H. Inoue, B. Kim, A. G. Swartz, T. A. Merz, Y. Hikita, S. Harashima, H. K. Sato, M. Minohara, S. Hoffmann-Eifert, R. Dittmann, and H. Y. Hwang, Phys. Rev. X **6**, 031035 (2016).

[4] H. R. Zhang, Y. Zhang, H. Zhang, J. Zhang, X. Shen, X. X. Guan, Y. Z. Chen, R. C. Yu, N. Pryds, Y. S. Chen, B. G. Shen, and J. R. Sun, Phys. Rev. B **96**, 195167 (2017).

[5] Y. Gan, Y. Zhang, D. V. Christensen, N. Pryds, and Y. Chen, Phys. Rev. B **100**, 125134 (2019).

[6] D. V. Christensen, Y. Frenkel, Y. Z. Chen, Y. W. Xie, Z. Y. Chen, Y. Hikita, A. Smith, L. Klein, H. Y. Hwang, N. Pryds, and B. Kalisky, Nat. Phys. **15**, 269 (2019).

[7] J. Zhang, H. Zhang, H. Zhang, Y. Ma, X. Chen, F. Meng, S. Qi, Y. Chen, F. Hu, Q. Zhang, B. Liu, B. Shen, W. Zhao, W. Han, and J. Sun, ACS Appl. Mater. Interfaces **12**, 28775 (2020).

[8] N. Lebedev, M. Stehno, A. Rana, P. Reith, N. Gauquelin, J. Verbeeck, H. Hilgenkamp, A. Brinkman, and J. Aarts, Sci. Rep. **11**, 10726 (2021).

[9] D.-S. Park, A. D. Rata, I. V. Maznichenko, S. Ostanin, Y. L. Gan, S. Agrestini, G. J. Rees, M. Walker, J. Li, J. Herrero-Martin, G. Singh, Z. Luo, A. Bhatnagar, Y. Z. Chen, V. Tileli, P. Muralt, A. Kalaboukhov, I. Mertig, K. Dörr, A. Ernst *et al.*, Nat. Commun. **11**, 3650 (2020).

[10] A. Joshua, S. Pecker, J. Ruhman, E. Altman, and S. Ilani, Nat. Commun. **3**, 1129 (2012).

[11] J. Ruhman, A. Joshua, S. Ilani, and E. Altman, Phys. Rev. B **90**, 125123 (2014).

[12] M. Diez, A. M. R. V. L. Monteiro, G. Mattoni, E. Cobanera, T. Hyart, E. Mulazimoglu, N. Bovenzi, C. W. J. Beenakker, and A. D. Caviglia, Phys. Rev. Lett. **115**, 016803 (2015).

[13] G. M. De Luca, R. Di Capua, E. Di Gennaro, F. M. Granozio, D. Stornaiuolo, M. Salluzzo, A. Gadaleta, I. Pallecchi, D. Marrè, C. Piamonteze, M. Radovic, Z. Ristic, and S. Rusponi, Phys. Rev. B **89**, 224413 (2014).

[14] C.-L. Chien, S. DeBenedetti, and F. D. S. Barros, Phys. Rev. B **10**, 3913 (1974).

[15] T. R. McGuire, M. W. Shafer, R. J. Joenk, H. A. Alperin, and S. J. Pickart, J. Appl. Phys. (Melville, NY) **37**, 981 (1966).

[16] J. Schiemer, L. J. Spalek, S. S. Saxena, C. Panagopoulos, T. Katsufuji, A. Bussmann-Holder, J. Köhler, and M. A. Carpenter, Phys. Rev. B **93**, 054108 (2016).

[17] A. Bussmann-Holder, J. Köhler, R. K. Kremer, and J. M. Law, Phys. Rev. B **83**, 212102 (2011).

[18] D. Bessas, K. Z. Rushchanskii, M. Kachlik, S. Disch, O. Gourdon, J. Bednarcik, K. Maca, I. Sergueev, S. Kamba, M. Ležaić, and R. P. Hermann, Phys. Rev. B **88**, 144308 (2013).

[19] D. S. Ellis, H. Uchiyama, S. Tsutsui, K. Sugimoto, K. Kato, D. Ishikawa, and A. Q. R. Baron, Phys. Rev. B **86**, 220301(R) (2012).

[20] T. Katsufuji and H. Takagi, Phys. Rev. B **64**, 054415 (2001).

[21] T. Katsufuji and Y. Tokura, Phys. Rev. B **60**, R15021 (1999).

[22] K. S. Takahashi, M. Onoda, M. Kawasaki, N. Nagaosa, and Y. Tokura, Phys. Rev. Lett. **103**, 057204 (2009).

[23] K. Tanaka, K. Fujita, Y. Maruyama, Y. Kususe, H. Murakami, H. Akamatsu, Y. Zong, and S. Murai, J. Mater. Res. **28**, 1031 (2013).

[24] S. C. Chae, Y. J. Chang, D.-W. Kim, B. W. Lee, I. Choi, and C. U. Jung, J. Electroceram. **22**, 216 (2009).

[25] K. Hatabayashi, T. Hitosugi, Y. Hirose, X. Cheng, T. Shimada, and T. Hasegawa, Jpn. J. Appl. Phys. **48**, 100208 (2009).

[26] K. Fujita, N. Wakasugi, S. Murai, Y. Zong, and K. Tanaka, Appl. Phys. Lett. **94**, 062512 (2009).

[27] K. Shimamoto, K. Hatabayashi, Y. Hirose, S. Nakao, T. Fukumura, and T. Hasegawa, Appl. Phys. Lett. **102**, 042902 (2013).

[28] K. Kugimiya, K. Fujita, K. Tanaka, and K. Hirao, J. Magn. Magn. Mater. **310**, 2268 (2007).

[29] K. Jiang, R. Zhao, P. Zhang, Q. Deng, J. Zhang, W. Li, Z. Hu, H. Yang, and J. Chu, Phys. Chem. Chem. Phys. **17**, 31618 (2015).

[30] H.-H. Wang, A. Fleet, J. D. Brock, D. Dale, and Y. Suzuki, J. Appl. Phys. (Melville, NY) **96**, 5324 (2004).

[31] R. Zhao, W. W. Li, L. Chen, Q. Q. Meng, J. Yang, H. Wang, Y. Q. Wang, R. J. Tang, and H. Yang, Appl. Phys. Lett. **101**, 102901 (2012).

[32] See Supplemental Material at http://link.aps.org/supplemental/10.1103/PhysRevMaterials.6.075003 for various sets of additional data.

[33] A. Shkabko, C. Xu, P. Meuffels, F. Gunkel, R. Dittmann, A. Weidenkaff, and R. Waser, APL Mater. **1**, 052111 (2013).

[34] A. Brinkman, M. Huijben, M. van Zalk, J. Huijben, U. Zeitler, J. C. Maan, W. G. van der Wiel, G. Rijnders, D. H. A. Blank, and H. Hilgenkamp, Nat. Mater. **6**, 493 (2007).

[35] F. Trier, D. V. Christensen, and N. Pryds, J. Phys. D: Appl. Phys. **51**, 293002 (2018).

[36] E. Mikheev, B. Himmetoglu, A. P. Kajdos, P. Moetakef, T. A. Cain, C. G. Van de Walle, and S. Stemmer, Appl. Phys. Lett. **106**, 062102 (2015).

[37] D. Stornaiuolo, B. Jouault, E. Di Gennaro, A. Sambri, M. D'Antuono, D. Massarotti, F. M. Granozio, R. Di Capua, G. M. De Luca, G. P. Pepe, F. Tafuri, and M. Salluzzo, Phys. Rev. B **98**, 075409 (2018).

[38] J. Smit, Physica (Amsterdam) **21**, 877 (1955).

[39] J. Smit, Physica (Amsterdam) **24**, 39 (1958).

[40] N. Nagaosa, J. Sinova, S. Onoda, A. H. MacDonald, and N. P. Ong, Rev. Mod. Phys. **82**, 1539 (2010).

[41] J. H. Lee, X. Ke, N. J. Podraza, L. F. Kourkoutis, T. Heeg, M. Roeckerath, J. W. Freeland, C. J. Fennie, J. Schubert, D. A.

[42] Muller, P. Schiffer, and D. G. Schlom, Appl. Phys. Lett. **94**, 212509 (2009).

[42] K. S. Takahashi, H. Ishizuka, T. Murata, Q. Y. Wang, Y. Tokura, N. Nagaosa, and M. Kawasaki, Sci. Adv. **4**, eaar7880 (2018).

[43] Y. Lin, E.-M. Choi, P. Lu, X. Sun, R. Wu, C. Yun, B. Zhu, H. Wang, W. Li, T. Maity, and J. MacManus-Driscoll, ACS Appl. Mater. Interfaces **12**, 8513 (2020).

[44] H. Akamatsu, K. Fujita, Y. Zong, N. Takemoto, S. Murai, and K. Tanaka, Phys. Rev. B **82**, 224403 (2010).

[45] H. Shin, C. Liu, F. Li, R. Sutarto, B. A. Davidson, and K. Zou, Phys. Rev. B **101**, 214105 (2020).

[46] M. Ben Shalom, C. W. Tai, Y. Lereah, M. Sachs, E. Levy, D. Rakhmilevitch, A. Palevski, and Y. Dagan, Phys. Rev. B **80**, 140403(R) (2009).

[47] M. Lee, J. R. Williams, S. Zhang, C. D. Frisbie, and D. Goldhaber-Gordon, Phys. Rev. Lett. **107**, 256601 (2011).

[48] D. Fuchs, A. Sleem, R. Schäfer, A. G. Zaitsev, M. Meffert, D. Gerthsen, R. Schneider, and H. v. Löhneysen, Phys. Rev. B **92**, 155313 (2015).

[49] J. Biscaras, S. Hurand, C. Feuillet-Palma, A. Rastogi, R. C. Budhani, N. Reyren, E. Lesne, J. Lesueur, and N. Bergeal, Sci. Rep. **4**, 6788 (2015).

[50] C. Yin, A. E. M. Smink, I. Leermakers, L. M. K. Tang, N. Lebedev, U. Zeitler, W. G. van der Wiel, H. Hilgenkamp, and J. Aarts, Phys. Rev. Lett. **124**, 017702 (2020).

[51] K. Bethe, Philips Research Rep. Suppl. **2**, 56 (1970).

[52] O. G. Vendik, E. K. Hollmann, A. B. Kozyrev, and A. M. Prudan, J. Supercond. **12**, 325 (1999).

[53] R. C. Neville, B. Hoeneisen, and C. A. Mead, J. Appl. Phys. (Melville, NY) **43**, 2124 (1972).

[54] J. Biscaras, N. Bergeal, S. Hurand, C. Grossetête, A. Rastogi, R. C. Budhani, D. LeBoeuf, C. Proust, and J. Lesueur, Phys. Rev. Lett. **108**, 247004 (2012).

[55] Y. Yan, L. Guo, L. Li, L. Wei, W. Chen, C. Zeng, and J. Hou, Phys. Rev. B **101**, 035119 (2020).

[56] M. M. Parish and P. B. Littlewood, Nature (London) **426**, 162 (2003).

[57] T. Khouri, U. Zeitler, C. Reichl, W. Wegscheider, N. E. Hussey, S. Wiedmann, and J. C. Maan, Phys. Rev. Lett. **117**, 256601 (2016).

[58] J. Hu, M. M. Parish, and T. F. Rosenbaum, Phys. Rev. B **75**, 214203 (2007).

[59] F. Kisslinger, C. Ott, and H. B. Weber, Phys. Rev. B **95**, 024204 (2017).

[60] N. Ramakrishnan, Y. T. Lai, S. Lara, M. M. Parish, and S. Adam, Phys. Rev. B **96**, 224203 (2017).

[61] T. Schumann, M. Goyal, D. A. Kealhofer, and S. Stemmer, Phys. Rev. B **95**, 241113(R) (2017).

[62] J. Xu, M. K. Ma, M. Sultanov, Z.-L. Xiao, Y.-L. Wang, D. Jin, Y.-Y. Lyu, W. Zhang, L. N. Pfeiffer, K. W. West, K. W. Baldwin, M. Shayegan, and W.-K. Kwok, Nat. Commun. **10**, 287 (2019).

[63] N. Lebedev, M. Stehno, A. Rana, N. Gauquelin, J. Verbeeck, A. Brinkman, and J. Aarts, J. Phys.: Condens. Matter **33**, 055001 (2020).

[64] A. E. M. Smink, J. C. de Boer, M. P. Stehno, A. Brinkman, W. G. van der Wiel, and H. Hilgenkamp, Phys. Rev. Lett. **118**, 106401 (2017).